Journal of Biomechanics 45 (2012) 371–381

Contents lists available at SciVerse ScienceDirect

Journal of Biomechanics

journal homepage: www.elsevier.com/locate/jbiomech
www.JBiomech.com

Effect of the fluid–structure interactions on low-density lipoprotein transport within a multi-layered arterial wall

Stephen Chung, Kambiz Vafai *

Department of Mechanical Engineering, University of California, Riverside (UCR), Riverside, CA 92521, USA

ARTICLE INFO

Article history:
Accepted 4 October 2011

Keywords:
Low-density lipoprotein transport
Fluid–structure interaction
Arterial wall
Porous media
Pulsation

ABSTRACT

The effects of fluid–structure interactions (FSI) and pulsation on the transport of low-density lipoprotein (LDL) through an arterial wall are analyzed in this work. To this end, a comprehensive multi-layer model for both LDL transport as well as fluid–structure interaction (FSI) is introduced. The constructed model is analyzed and compared with the existing results in the limiting cases. Excellent agreement is found between the presented model and the existing results in the limiting cases. The presented model takes into account the complete multi-layered LDL transport while incorporating the FSI aspects to enable a comprehensive study of the deformation effect on the pertinent parameters of the transport processes within an artery. Since the flow inside an artery is time-dependent, the impact of pulsatile flow is also analyzed with and without FSI. A detailed analysis is presented to illustrate the consequence of different factors on the LDL transport in an artery.

1. Introduction

Atherosclerosis and cardiovascular topics have been studied by many researchers due to its broad impact on the longevity and mortality of the population at large. Existence of higher concentration of macromolecules, mainly low-density lipoprotein (LDL) is an important factor in the initiation of atherosclerosis. To understand and assess the impact of LDL transport on atherosclerosis, a comprehensive model, which is capable of displaying the transport phenomena within different layers of the arterial wall, is required.

One of the earlier models for transport inside a blood vessel was presented by Prosi et al. (2005). They introduced two primary models. These were wall-free and lumen-wall models. These models, are widely used to study mass transfer within arteries (Rappitsch and Perktold, 1996; Wada and Karino, 2000; Moore and Ethier, 1997; Stangeby and Ethier, 2002a,b). It is more appropriate to treat the arterial wall as non-homogenous, since each of the layers posses a different structure. For example, endothelium, a thin layer between intima and lumen, has a role in reducing disturbances in the blood flow, while adventitia is a thicker gel layer that attaches to organs to stabilize the artery's position. In general, the hydraulic, mass transport, and elastic properties for these different layers are different. As such a multi-layer model is much more realistic. Several aspects related to the macro-scale (Huang et al., 1994; Tada and Tarbell, 2004) as well as micro-scale (Fry, 1985; Karner et al., 2001; Yuan et al., 1991; Weinbaum et al., 1992; Wen et al., 1988) features will be incorporated within our model.

To describe the mass transfer inside a low permeability porous media, the traditional Staverman–Kedem–Katchalsky membrane equation (Kedem and Katchalsky, 1958) is usually invoked. Built on a steady state assumption, this equation might not be appropriate for a time dependent process such as when the effect of pulsation is taken into account. Yang and Vafai (2006, 2008) and Ai and Vafai (2006) had developed a comprehensive new four-layer model, where endothelium, intima, internal elastic lamina (IEL), and media are all treated as different layers macroscopically. Porous media approach has been utilized based on volume averaging theorems to establish the governing equations while accounting for the Staverman filtration and osmosis effects.

In Yang and Vafai (2006, 2008) and Ai and Vafai's (2006) works, details of the interactions between lumen and arterial wall were analyzed, and Staverman filtration and osmotic reflection were incorporated in their model to account for selective permeability. The development of homogeneous properties in each of the layers was discussed and obtained based on microscopic structure of different membranes (Huang et al., 1992, 1997; Huang and Tarbell, 1997; Karner et al., 2001) or the available experimental data utilizing a circuit analogy model (Prosi et al., 2005; Ai and Vafai, 2006). The effect of adventitia was embedded within the flux (or concentration) condition located at the outer boundary of media. Glycocalyx, a very thin layer that covers and separates endothelium from lumen region was found to be negligible (Michel and Curry, 1999; Tarbell, 2003).

Most of the earlier works treat the arterial wall as a solid non-elastic medium, which does not represent the real physiological condition. The arterial wall, is an elastic bio-material, which will

* Corresponding author. Tel.: +1 951 827 2135; fax: +1 951 827 2899.
E-mail address: vafai@engr.ucr.edu (K. Vafai).

0021-9290/$ - see front matter © 2011 Elsevier Ltd. All rights reserved.
doi:10.1016/j.jbiomech.2011.10.002

Nomenclature

c	LDL concentration
$\ddot{d}_s$	acceleration within the solid region
D	LDL diffusivity
f_s	solid domain body force
H	thickness of the layers
k	reaction coefficient
K	permeability
L	length of the artery
L_{end}	thickness of the endothelium layer
N''	solute mass flux per area
p	hydraulic pressure
Δp	pressure drop across arterial wall
Δp^*	time-dependent pressure drop across arterial wall
Pe	Peclet number
r_m	molecular radius
R_{Cell}	radius of endothelial cell
R	radius of lumen domain
t	time
T	pulsation period
u	axial velocity
$\vec{u}$	velocity vector
U	maximum velocity at entrance
U^*	time-dependent maximum velocity at entrance
v	filtration velocity
w	half width of the leaky junction
α_{lj}	r_m/w
β	ratio of the pore deformation to the wall deformation
γ	sieving coefficient$(1-\sigma)$
δ	porosity
ε	angular strain
ϕ	fraction of cells with leaky junction
μ	viscosity
ρ	fluid density
ρ_s	membrane density
σ_s	Cauchy stress tensor
σ	reflection coefficient

Subscripts

70 mmHg	refers to properties with a gage pressure of 70 mmHg
eff	refers to effective property
end	refers to endothelium layer
lj	refers to leaky junction
nj	refers to normal junction

deform due to the pressure difference across the arterial wall. Furthermore, this deformation changes in time since the pressure applied from lumen side is affected by the pulsation of cardiovascular system. Gao et al. (2006a,b) performed a numerical simulation on the stress distribution across the aorta wall. Based on the work of Gao et al. (2006a,b), which considers zero pressure at the outlet of aorta, Khanafer and Berguer (2009) introduced a more realistic model by applying time-dependent pressure in a wave-form. Utilizing the fluid–structure interaction (FSI) model, Khanafer et al. (2009) further analyzed the turbulent flow effect and the wall stress on aortic aneurysm.

The current work presents a model that couples the multi-layer model for LDL transport while fully incorporating the FSI effects. The change of hydraulic and mass transfer properties due to the wall deformation is analyzed, and its effect on flow and LDL transport through the arterial wall is investigated. Furthermore, the impact of pulsatile flow is studied along with its effect on the LDL transport within an arterial wall.

2. Formulation

2.1. Multi-layer model

A typical structure of the wall for an artery can be represented by six layers as shown in Fig. 1. These layers are, moving away from the lumen, glycocalyx, endothelium, intima, internal elastic lamina (IEL), media, and adventitia. As mentioned earlier, glycocalyx will not be considered due to its negligible thickness (Yang and Vafai, 2006, 2008; Ai and Vafai, 2006). The endothelium is a thin layer attached at the inner side of artery, which protects the arterial wall from the inner side and reduces the blood flow disturbances. Next, intima allows flexibility within the arterial wall, while the internal elastic lamina is a thin low-permeability layer connecting intima and media. Media is a layer with capillaries passing through it and surrounded by adventitia, a gel-like layer, which stabilizes the artery by connecting it to an adjacent organ.

The lumen domain is considered as a cylindrical geometry with radius of R and axial length L. Surrounding the lumen, the thickness and properties of each layer of arterial wall is shown in Table 1, where the data for endothelium, intima, IEL, and media (Prosi et al., 2005; Karner et al., 2001) is utilized (Yang and Vafai, 2006, 2008; Ai and Vafai, 2006).

2.2. Governing equations

In the lumen part, the flow can be described by the Navier–Stokes equation. The governing equations for conservation of mass, momentum and species are

$$\nabla\cdot\vec{u}=0$$
$$\rho\frac{D\vec{u}}{Dt}=-\nabla p+\mu\nabla^2\vec{u}$$
$$\frac{\partial c}{\partial t}+\vec{u}\cdot\nabla c=D\nabla^2 c \quad (1)$$

where $\vec{u}$ is the velocity vector, c the LDL concentration, p the hydraulic pressure, and ρ, μ, and D are the fluid density, viscosity, and diffusivity coefficient, respectively.

The hydraulic and mass transfer characteristics of adventitia are represented by a boundary condition at its outer layer (Yang and Vafai, 2006, 2008; Ai and Vafai's, 2006). The flow and mass transfer governing equations within the four layers, endothelium, intima, IEL, and media, can be represented by

$$\nabla\cdot\vec{u}=0$$
$$\frac{\rho}{\delta}\frac{\partial\vec{u}}{\partial t}+\frac{\mu_{eff}}{K}\vec{u}=-\nabla p+\mu_{eff}\nabla^2\vec{u}$$
$$\frac{\partial c}{\partial t}+(1-\sigma)\vec{u}\cdot\nabla c=D_{eff}\nabla^2 c-kc \quad (2)$$

where δ is the porosity, μ_{eff} the effective fluid viscosity, K the permeability, σ the reflection coefficient, D_{eff} the effective LDL diffusivity, k the reaction coefficient, which is non-zero only inside the media layer and is zero for the other layers (Prosi et al., 2005; Yang and Vafai, 2006, 2008). The properties for each of the layers is listed in Table 1, where the endothelium properties change with deformation as elaborated later on in this work.

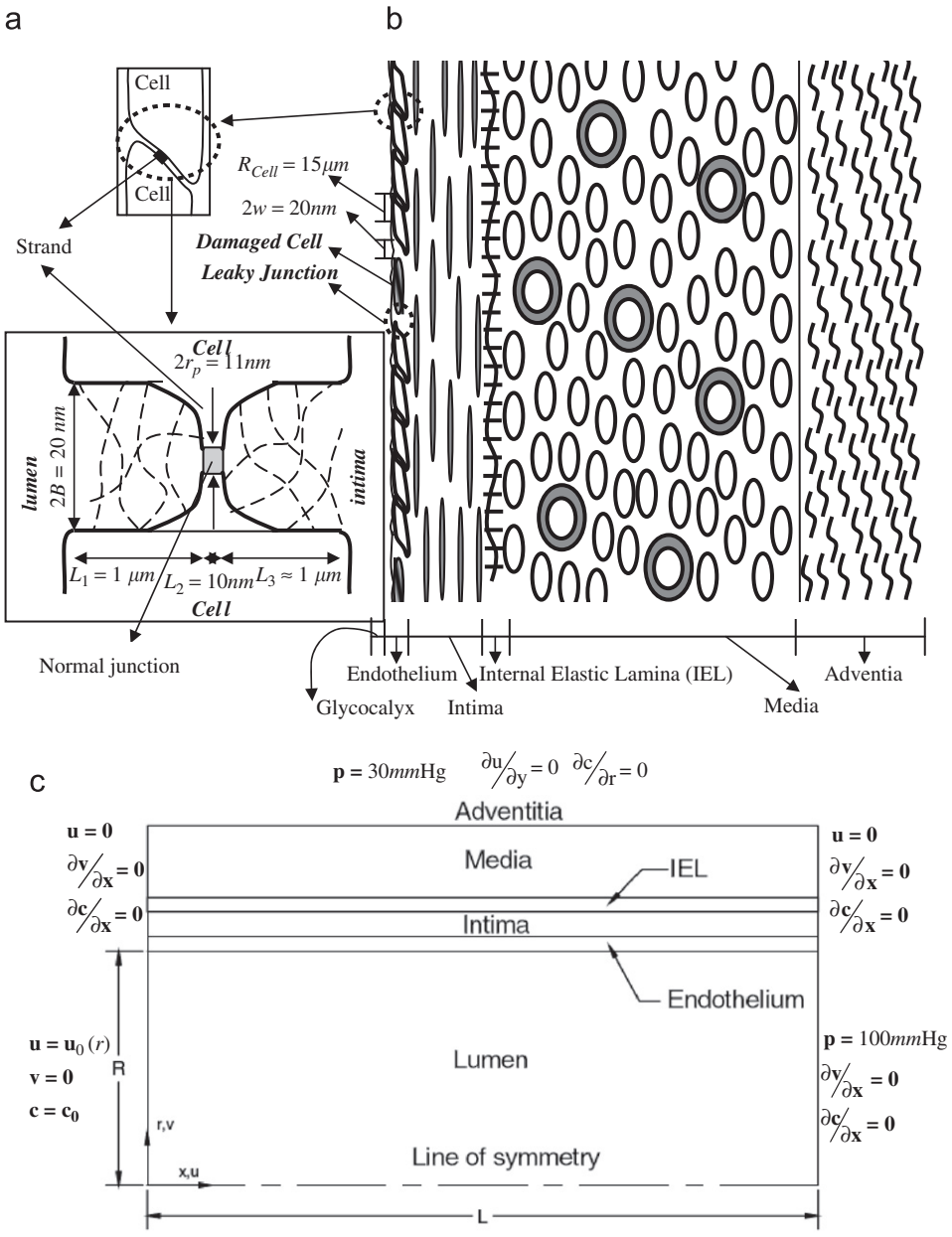

Fig. 1. Configuration of (a) junction, (b) arterial wall, and (c) computation domain.

Table 1
Parameters used in the numerical simulation (Yang and Vafai 2006, 2008; Khanafer and Berguer, 2009).

	Lumen	Endothelium	Intima	IEL	Media	Adventitia
Density, ρ (kg/mm^3)	1.07×10^3	1.057×10^3	1.057×10^3	1.057×10^3	1.057×10^3	1.057×10^3
Diffusivity, D_{eff} (m^2/s)	2.87×10^{-11}	5.7061×10^{-18}[a]	5.4×10^{-12}	3.18×10^{-15}	5×10^{-14}	
Elasticity (MPa)		2	2	2	6	4
Permeability K (m^2)		3.22×10^{-21}[a]	2×10^{-16}	4.392×10^{-19}	2×10^{-18}	
Porosity, δ		5×10^{-4}	0.983	0.002	0.258	
Reaction coefficient, k (s^{-1})	0	0	0	0	3.197×10^{-4}	
Refection coefficient, σ		0.9888[a]	0.8272	0.9827	0.8836	
Thickness, H (μm)	3100	2	10	2	200	100
Viscosity,μ_{eff} (kg/m s)	3.7×10^{-3}	0.72×10^{-3}	0.72×10^{-3}	0.72×10^{-3}	0.72×10^{-3}	

[a] Parameters with gage pressure of 70 mmHg and adjusted based on deformation of endothelium for different gage pressures.

A hyper-elastic model is used to describe the elastic structure of the artery. The elastodynamic equation can be written as

$$\rho_s \ddot{d}_s = \nabla\sigma_s + f_s \tag{3}$$

where ρ_s is the density, $\ddot{d}_s$ the acceleration within the solid region, f_s the solid domain body force, and σ_s the Cauchy stress tensor, where the Mooney–Rivlin material model is invoked to describe the strain–energy relationship.

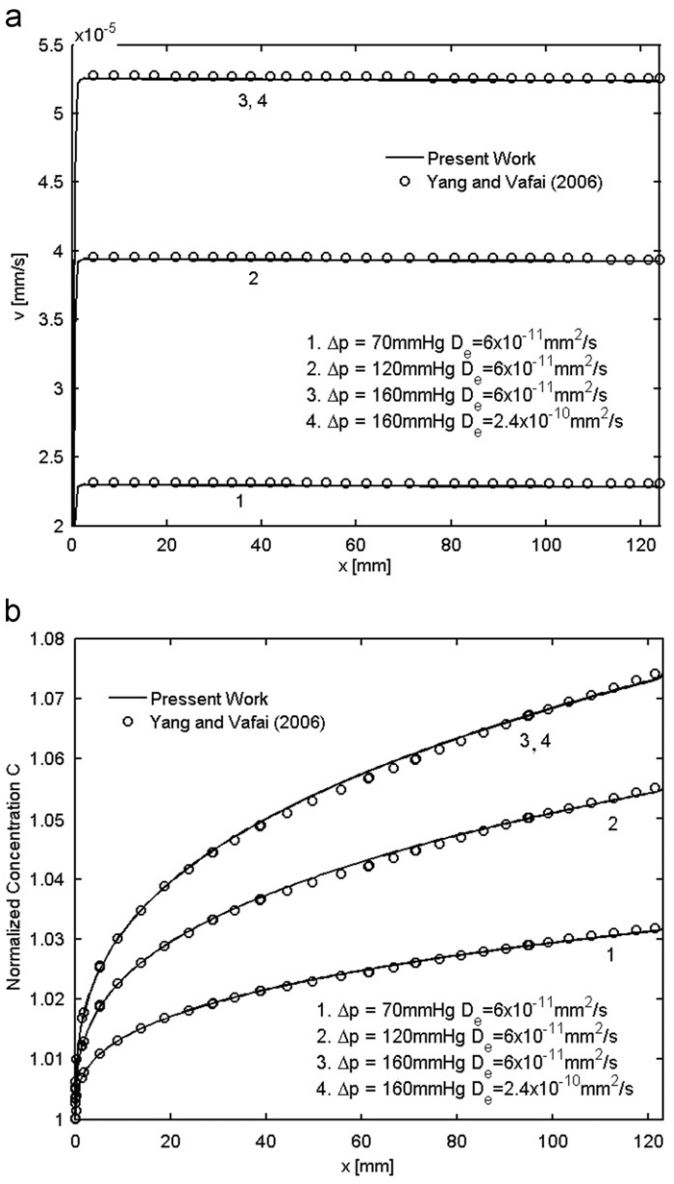

Fig. 2. Comparison of (a) filtration velocity and (b) LDL concentration at lumen–endothelium interface with those of Yang and Vafai (2006).

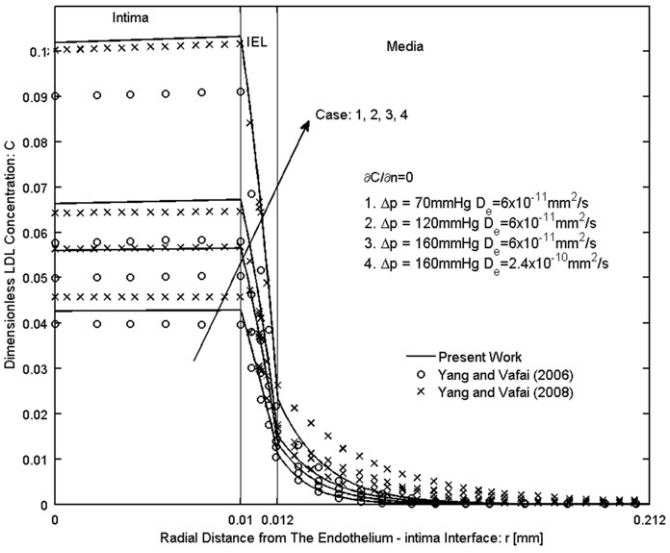

Fig. 3. Comparison of normalized LDL concentration across intima, IEL, and media at different gage pressures and effective diffusivity with (a) numerical and (b) analytical results of Yang and Vafai (2006, 2008).

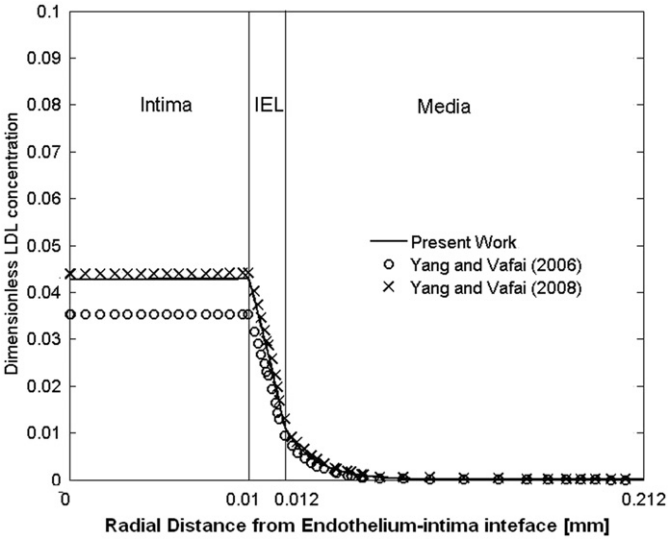

Fig. 4. Comparison of normalized LDL concentration across intima, IEL, and media with numerical and analytical results by Yang and Vafai (2006, 2008).

2.3. Boundary conditions

The boundary conditions are shown in Fig. 1, where the entrance velocity is expressed as

$$u = U^*(1-(r/R)^2) \quad at \;\; x=0,\; 0 \le r \le R \tag{4a}$$

where $U^* = U(1+\sin(2\pi t/T))$, and the pressure drop across the lumen and the arterial wall is expressed as

$$\Delta p^* = \Delta p + 25\sin(2\pi t/T) \tag{4b}$$

The nominal maximum entrance velocity and pressure drop through the arterial wall, U and Δp, are taken as 0.338 m/s and 70 mm Hg for the steady state case. For a pulsatile flow with a time period of $T=1$ s, U^* and Δp^* dependency on time can be presented as $0.338(1+\sin(2\pi t/T))(m/s)$ and $70+25\sin(2\pi t/T)$ $(mmHg)$, respectively. LDL concentration at the entrance is taken as $c_0 = 28.6\times10^{-3}\,mol/m^3$. Jump conditions for momentum, mass transfer, and the elastic structure are invoked at the interface between each of the layers. The Staverman filtration is invoked when representing the continuity of LDL transport as

$$\left[(1-\sigma)uc - D\frac{\partial c}{\partial r}\right]\Big|_+ = \left[(1-\sigma)uc - D\frac{\partial c}{\partial r}\right]\Big|_- \tag{5}$$

2.4. Calculation of endothelium properties from the micro-structure attributes

Endothelium is a layer that causes the highest hydraulic and mass transfer resistance across the wall of an artery due to its small pore size. Therefore, the elastic deformation in the arterial wall will have much more impact on flow and mass transfer behavior within the endothelium layer. The pores of endothelium can be characterized as normal or leaky junction as shown in Fig. 1a. Normal junction is the space between strands, which connects the endothelial cells. Leaky junction is formed due to dysfunctional strands when the cells are damaged resulting in altered strands with a cross-sectional area, which is substantially larger than the normal junction.

Pore theorem is well accepted for calculating permeability, effective diffusivity, and reflection coefficient in the literature (Curry, 1984; Huang et al., 1992; Karner et al., 2001). Applying pore theorem, the endothelium permeability K_{end} can be expressed as

$$K_{end} = K_{lj} + K_{nj} \tag{6a}$$

$$K_{lj} = \frac{w^2}{3}\frac{4w\phi}{R_{Cell}} \tag{6b}$$

where w is the half-width of the leaky junction, R_{Cell} is the radius of the endothelial cell taken as 15 μm, and ϕ is the fraction of the leaky junction taken as 5×10^{-4} (Huang et al., 1992).

In this study, the normal junction is assumed to be impermeable for the LDL molecule ($D_{nj}=0$; $\sigma_{nj}=1$), since the average radius of the normal junction is 5.5 nm, which is smaller the radius of LDL molecule ($r_m=11$ nm). Therefore using the pore theorem and incorporating the effect of the tissue matrix, the effective diffusivity and reflection coefficients can be calculated as

$$D_{end} = D_{lj} = D_{free}(1-\alpha_{lj})(1-1.004\alpha_{lj}+0.418\alpha_{lj}^3-0.169\alpha_{lj}^5)\frac{4w}{R_{Cell}}\phi \tag{7}$$

$$\sigma_{end} = \frac{\sigma_{nj}K_{nj}+\sigma_{lj}K_{lj}}{K_{nj}+K_{lj}} = 1-\frac{(1-\sigma_{lj})K_{lj}}{K_{nj}+K_{lj}} \tag{8a}$$

$$\sigma_{lj} = 1-\left(1-\tfrac{3}{2}\alpha_{lj}^2+\tfrac{1}{2}\alpha_{lj}^3\right)\left(1-\tfrac{1}{3}\alpha_{lj}^2\right) \tag{8b}$$

where α_{lj} is the ratio of r_m to w.

Huang et al. (1992) and (Karner et al., 2001) specified the half width of the leaky junction as $w=10$ nm, which is the same as the cleft opening for a normal junction. This value of width is smaller than the radius of LDL particle, so leaky junction, by pore theorem, becomes impermeable to LDL molecule. However, when deformation occurs, realistically, without the connection of strands between cells, leaky junction should have a larger gap. As such, a more reasonable representation should be calculated based on the approach given by Ai and Vafai (2006).

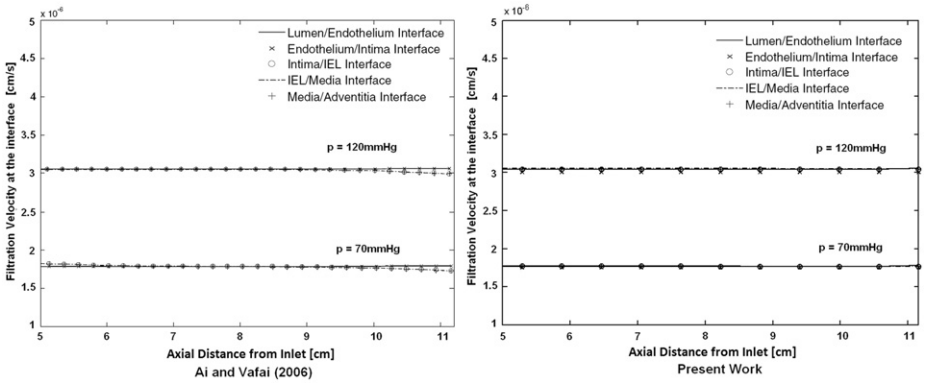

Fig. 5. Comparison of filtration velocity at different interfaces and axial location with those by Ai and Vafai (2006).

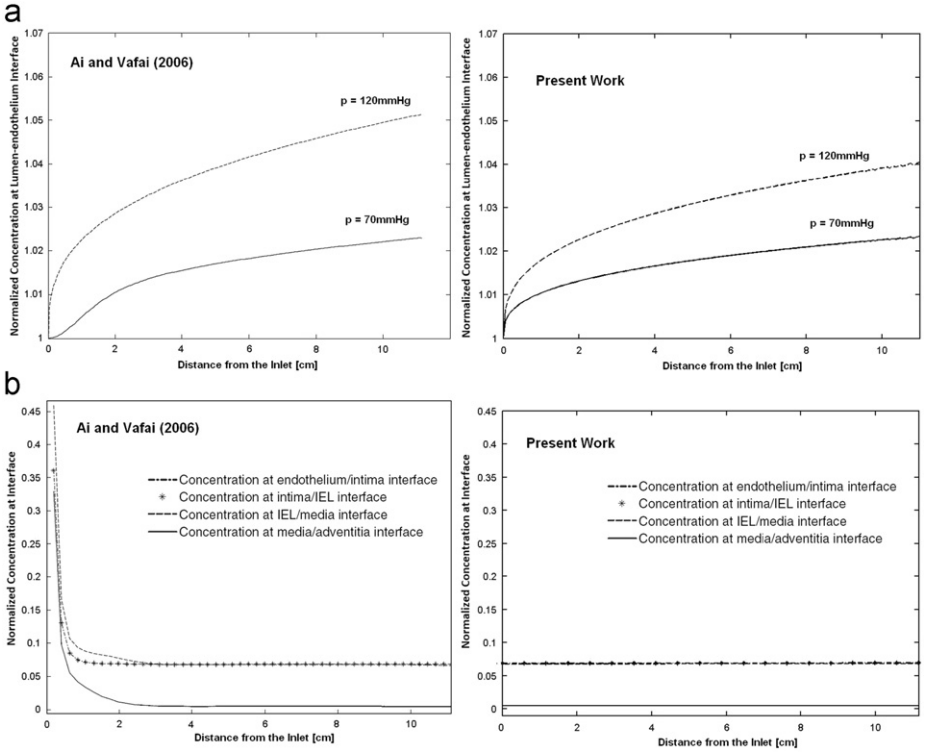

Fig. 6. Comparison of normalized LDL concentration at different interfaces and axial locations with those by Ai and Vafai (2006).

To obtain more realistic values of w, Ai and Vafai (2006) presented a logical approach through the application of circuit analogy to obtain

$$N''/c = \frac{D_{end} Pe_{end} \exp(Pe_{end})}{H_{end}(\exp(Pe_{end})-1)} \tag{9}$$

where N'' is solute mass flux per area, H_{end} thickness of endothelium, and the Peclet number for endothelium Pe_{end} can be expressed as

$$Pe_{end} = \frac{(1-\sigma_{end})H_{end}}{D_{end}} u \tag{10}$$

Further, in Ai and Vafai's (2006) work, the normal case corresponded to a lumen pressure of 100 mmHg, $N''/c = 2 \times 10^{-10}$ m/s, $u = 1.78 \times 10^{-8}$ m/s, and $K_{end} = 3.22 \times 10^{-21} m^2$ (Truskey et al., 1992; Meyer et al., 1996; Huang and Tarbell's, 1997). Solving Eqs. (6)–(10), results in the half width of the leaky junction as 14.343 nm, when the gage pressure is 70 mmHg. The properties of endothelium with gage pressure of 70 mmHg can be seen in Table 1, which is used as a reference value when calculating properties due to deformation.

2.5. Deformation-pore size ($\varepsilon - w$) relation

The $\theta-$ direction strain ε, obtained from the elastic equation, is considered to have a substantially more impact on the pore size w due to the pore shape and distribution. To correlate ε with w, a

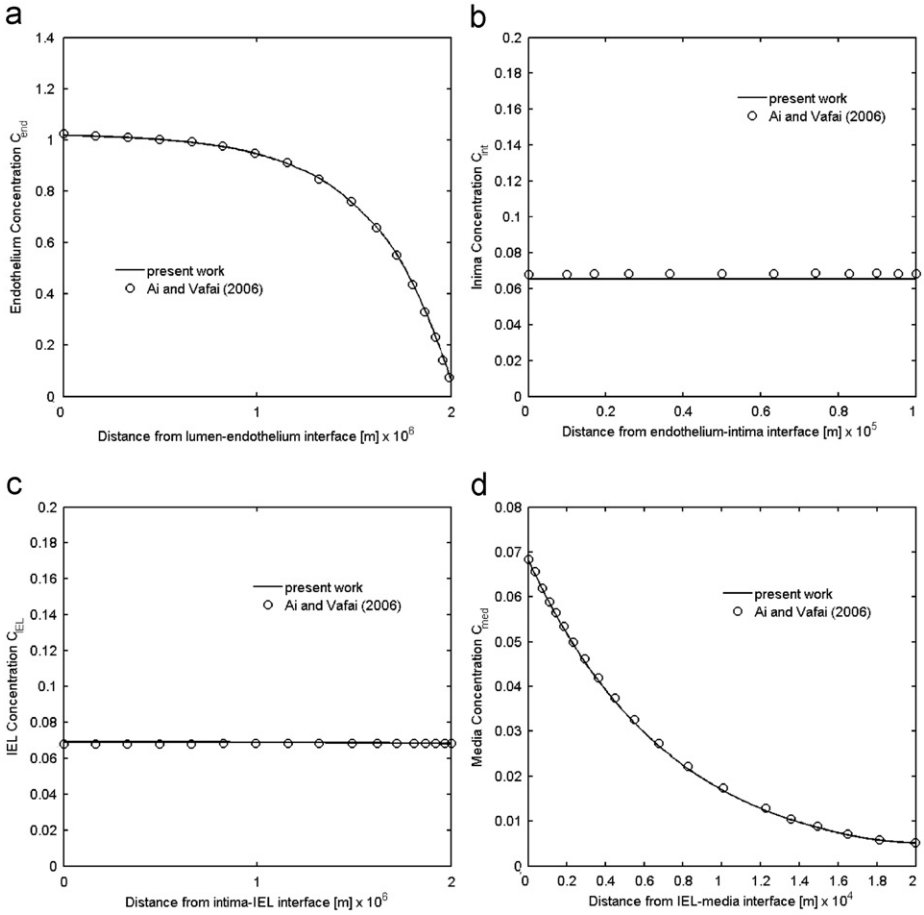

Fig. 7. Comparison of normalized LDL concentration across each of the layers with those by Ai and Vafai (2006).

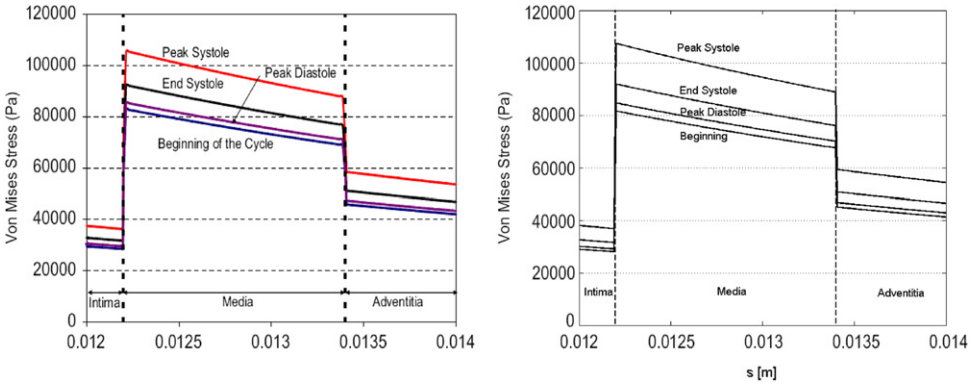

Fig. 8. Comparison of Von Mises stress across arterial wall at different steps in pulsation cycle with those by Khanafer and Berguer (2009).

coefficient β_{lj} is introduced as

$$\beta_{lj} = \frac{\varepsilon_{lj}}{\varepsilon} \tag{11}$$

where ε_{lj} is the expansion ratio of the leaky junction. Since cross-sectional area of the leaky junction is $2\pi R_{cell} w$, w can be considered as a function of ε:

$$w = w_{70\,\mathrm{mmHg}} \frac{1+\beta_{lj}\varepsilon}{1+\beta_{lj}\varepsilon_{70\,\mathrm{mmHg}}} \tag{12}$$

3. Methodology and validation

Comsol Multi-physics, software is used to solve the governing partial differential equations in this work. A detailed systematic set of runs were executed to ensure that the results are grid and time step independent with relative and absolute error of 10^{-3} and 10^{-6}, respectively. Our model and the computational results were validated through comparison with the available limiting cases in the literature. The LDL component was compared (Figs. 2–8) with the works of Yang and Vafai (2006, 2008) and Ai and Vafai (2006), while validation for FSI model (Figs. 9 and10) was done with the work of Khanafer and Berguer (2009).

Figs. 2 and 3 illustrate the comparisons with Yang and Vafai's (2006) work. As can be seen both the filtration velocity and LDL concentration are in very good agreement with Yang and Vafai's (2006) numerical results, which were obtained using an entirely different solution schemes. Comparisons of LDL concentration across intima, IEL and media with both numerical and analytical results of Yang and Vafai (2006, 2008) are demonstrated in Fig. 4. Once again a very good agreement is observed with only a very small difference near endothelium–intima interface. The present results are very close to those of Yang and Vafai (2006, 2008), especially to Yang and Vafai's analytical work (2008).

For further validation of computational results and LDL transport model within the multi-layers, another set of comparisons with Ai and Vafai's (2006) work are shown in Figs. 5–7. Filtration velocity and LDL concentration at endothelium–intima interface obtained in the present work are compared with those in an earlier study, resulting very good agreement as seen in Figs. 5 and 6. A perfect agreement can be seen in Fig. 7, for LDL concentration across each of the arterial layers against the results of Ai and Vafai (2006).

Fig. 8 displays Von Misses stress at different parts of the pulsation cycle across the arterial wall. Effects of higher value of elasticity across media are shown in Fig. 9 The present results are compared with those obtained by Khanafer and Berguer (2009), showing excellent agreement for the results presented in Figs. 8 and 9. Figs. 2–9 establish and validate different modules of the current models against available limiting cases in the literature covering both multilayer as well as the FSI attributes.

4. Results and discussion

4.1. FSI effect

Fig. 10 displays the variations of the half width of the leaky junction, w versus the angular strain, ε. This representation is based on Eq. (12), which shows that w increases linearly with an increase in ε. Larger β_{lj} produces a more substantial deformation of the pore size at larger values of ε, while reaching a limiting case at a certain value of ε, beyond which, w decreases as β_{lj} increases. Using Eqs. (6)–(11), the variations of pertinent properties such as endothelium's permeability, effective diffusivity, and reflection coefficient with ε are illustrated in Fig. 11. The effective properties for a higher fraction of leaky junction $\phi = 0.10\%$ are also shown in Fig. 11.

With respect to flow penetration, the permeability of a leaky junction is more than that of a normal junction permeability, which experiences a negligible change with deformation. However, the fraction of leaky junctions is much smaller than normal junction. On the other hand, LDL will mainly pass across the endothelium layer through a leaky junction, rather than a normal junction whose cross-section area is too small for LDL transport. Therefore, as can been seen in Fig. 11, variations in ε have a more pronounced impact on the effective diffusivity and reflection coefficient as compared to the permeability. To further illustrate the deformation effect on the reflection coefficient, the variations of the sieving coefficient $\gamma_{end} = (1-\sigma_{end})$ with the θ-strain ε are displayed in Fig. 11, showing how convection is affected by deformation. Fig. 11 confirms our physical expectations that endothelium is more permeable for both blood flow and LDL molecule transport for larger deformations. Also, as can be seen in Fig. 11, the endothelium becomes more permeable at a higher fraction of leaky junctions ϕ. This is due to the fact that a single

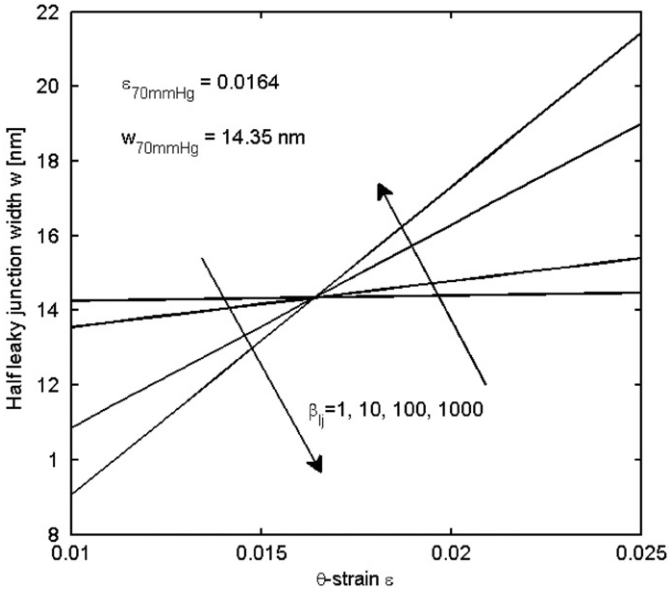

Fig. 10. Half width of leaky junction w variations with the angular strain ε.

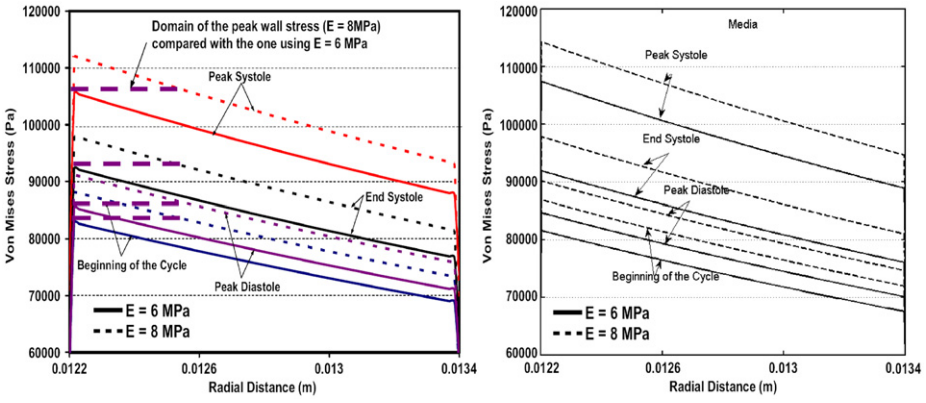

Fig. 9. Comparison of Von Mises stress across media at different steps in pulsation cycle and different elasticities with those by Khanafer and Berguer (2009).

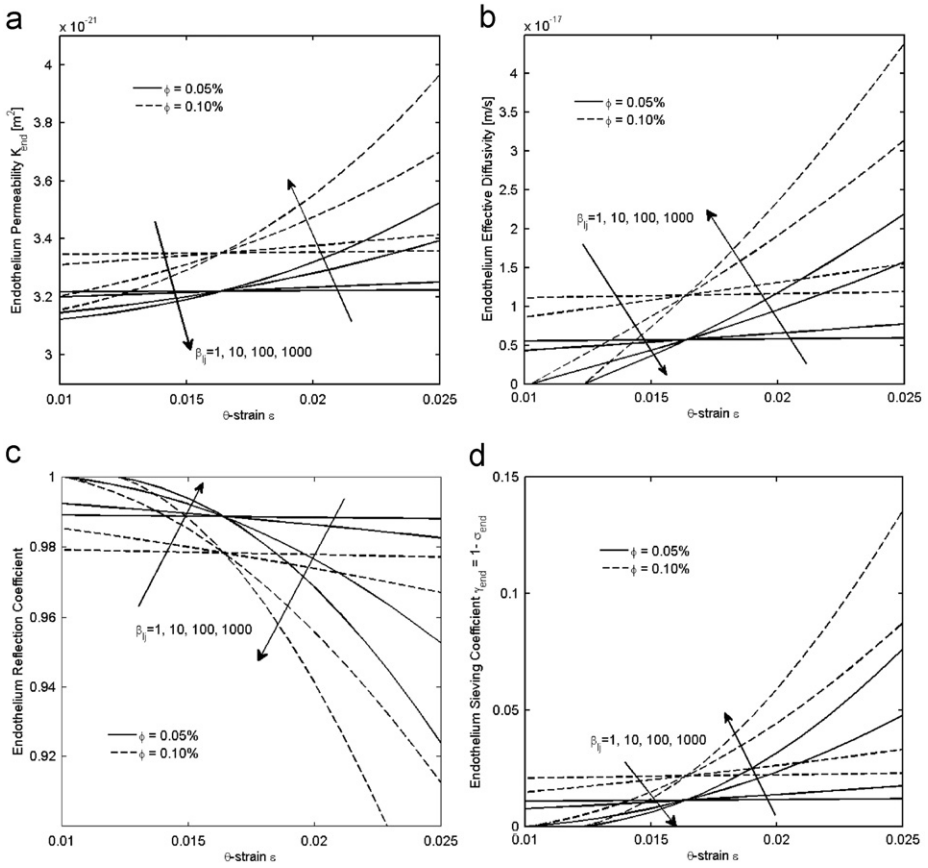

Fig. 11. Endothelium (a) permeability K_{end}, (b) effective diffusivity D_{eff}, (c) reflection coefficient σ_{end}, and (d) sieving coefficient γ_{end} $(=1-\sigma_{end})$, variations with angular strain ε at different ϕ and β_l .

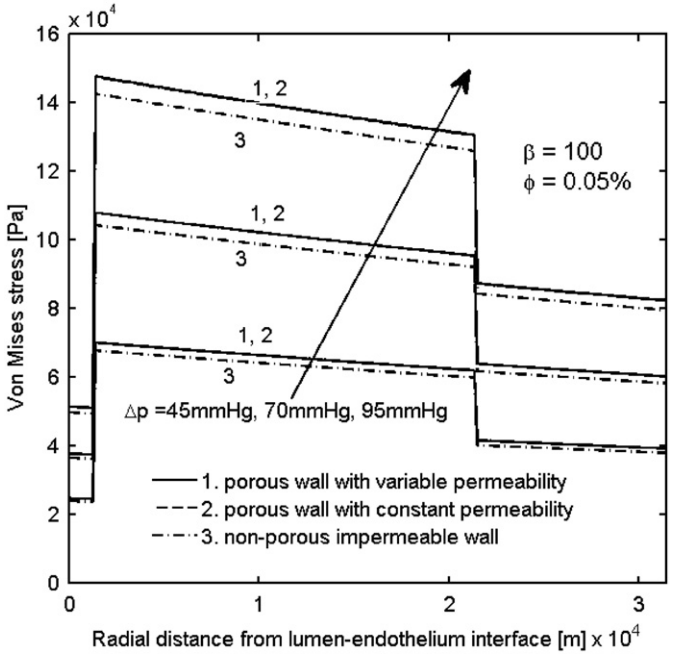

Fig. 12. Von Misses stress variations at the lumen–endothelium interface for different pressure drops across the arterial wall and different FSI models.

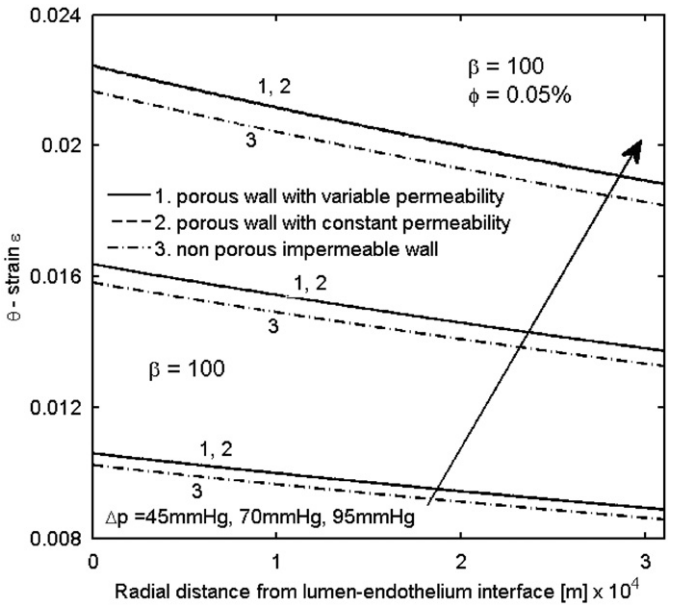

Fig. 13. Angular strain ε variations at the lumen–endothelium interface for different pressure drops across the arterial wall and different FSI models.

leaky junction has a substantially larger cross-sectional area than a single normal junction has.

Figs. 12 and 13 illustrate the angular strain and von Misses stress variations of the endothelium layer for different pressure drops across the lumen and the outer arterial wall. It can be seen that consideration of porous wall has a significant impact on the FSI results. On the other hand, variable permeability caused by deformed pores has a minor influence on the elastic behavior of the arterial wall due to a small fraction of leaky junctions (ϕ=0.05% and 0.10%). The filtration and concentration

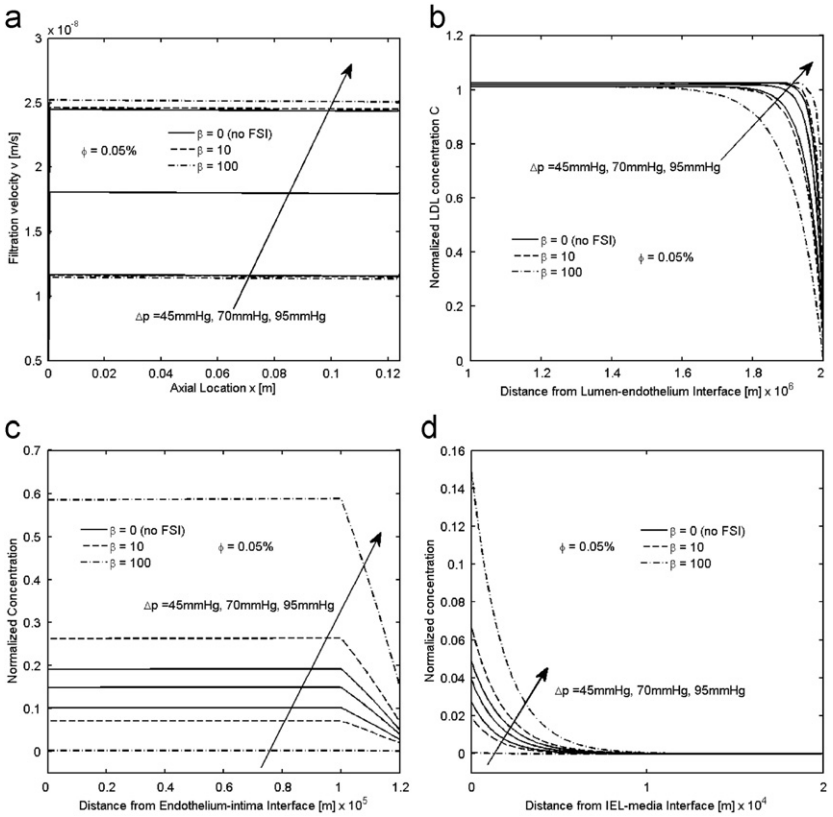

Fig. 14. (a) Filtration velocity variations at the lumen–endothelium interface, and normalized LDL concentration across (b) endothelium, (c) intima and IEL, and (d) media, for different β and Δp.

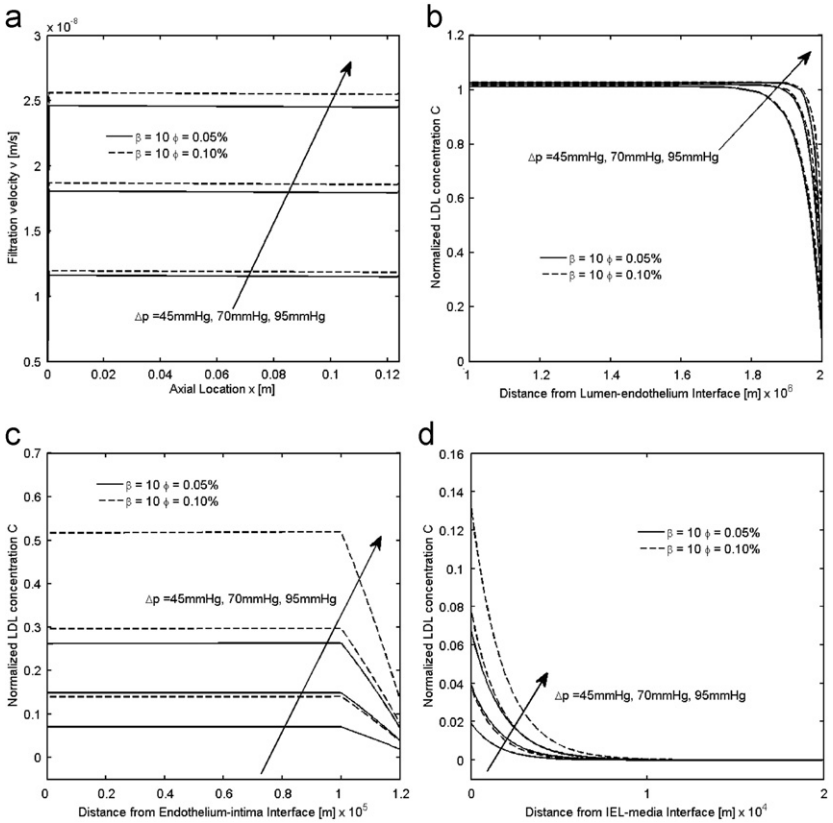

Fig. 15. (a) Filtration velocity variations at the lumen–endothelium interface, and normalized LDL concentration across (b) endothelium, (c) intima and IEL, and (d) media, for different ϕ and Δp.

distributions within different layers, while accounting for FSI effects and variable permeability, diffusivity and reflection coefficient at different pressure levels are shown in Fig. 14. The results of angular strain ε are then incorporated with those in Fig. 11, resulting the flow penetration and LDL concentration distributions shown in Fig. 14. Fig. 14(a) shows that the hydraulic pressure gradient dominates the flow penetration within different layers of an artery. FSI has a substantially more limited effect in enhancing the flow penetration in terms of creating a variable permeability and deformed leaky junction. This is because the deformation by FSI poses an insignificant effect, due to the limited flow through the leaky junction (ϕ=0.05% and 0.10%) as compared to that through the normal junction.

Fig. 14 also shows the impact of endothelium deformation on LDL transport for different pressure drops across lumen and the outer arterial wall. Since leaky junction affects the diffusion of LDL macromolecules, FSI has a more pronounced affect on the concentration distribution across different layers as seen in Fig.14. This is in contrast to the relatively insignificant effect of FSI on the filtration velocity. Fig. 14 clearly shows that FSI augments the impact of pressure change across the arterial wall. As can be seen in Fig. 14 the pressure and FSI effects are most significant within the intima layer. The impact of FSI becomes more pronounced as β_{lj} increases, due a larger cross-sectional area of a leaky junction.

As seen in Fig. 15, when ϕ increases from 0.05% to 0.10%, the permeability for blood flow as well as LDL transport increases, resulting in a higher value of filtration velocity and LDL concentration. Again this is due to the fact that a leaky junction has a much larger cross-sectional area than a normal junction, which allows more blood flow and LDL molecules through the endothelium layer. As φ increases, the impact of FSI becomes more pronounced, because the deformation of a leaky junction is significantly more than that of a normal junction.

4.2. Pulsation effect

Fig. 16 shows the impact of pulsation on the entrance velocity and pressure. As can be seen in Fig. 16, the pulsation has a more pronounced effect on the concentration distribution for larger values of pulsation period T. Also as can be seen in Fig. 16, incorporating pulsation for the pressure, increases the filtration velocity and concentration, while the velocity pulsation has an insignificant effect on the results. It should be noted that the impact of pulsation on LDL concentration is quite limited, due to the very dominant transient effect on mass transfer caused by the very small pulsation period ($(T=1$ s)).

Fig. 17 illustrates the FSI effect on filtration velocity when pulsation is taken into account. As was the case for the steady state results (Fig. 14a), FSI does not have a significant effect on the results since the leaky junction plays a minor role on the flow penetration. Fig. 18 shows that FSI has a negligible effect on the temporal concentration response in contrast to the FSI's significant effect on the steady state concentration distribution. The reason that FSI has a less pronounced effect on the concentration profile under pulsation, is due to the substantial damping effect of the pulsatile flow in an artery.

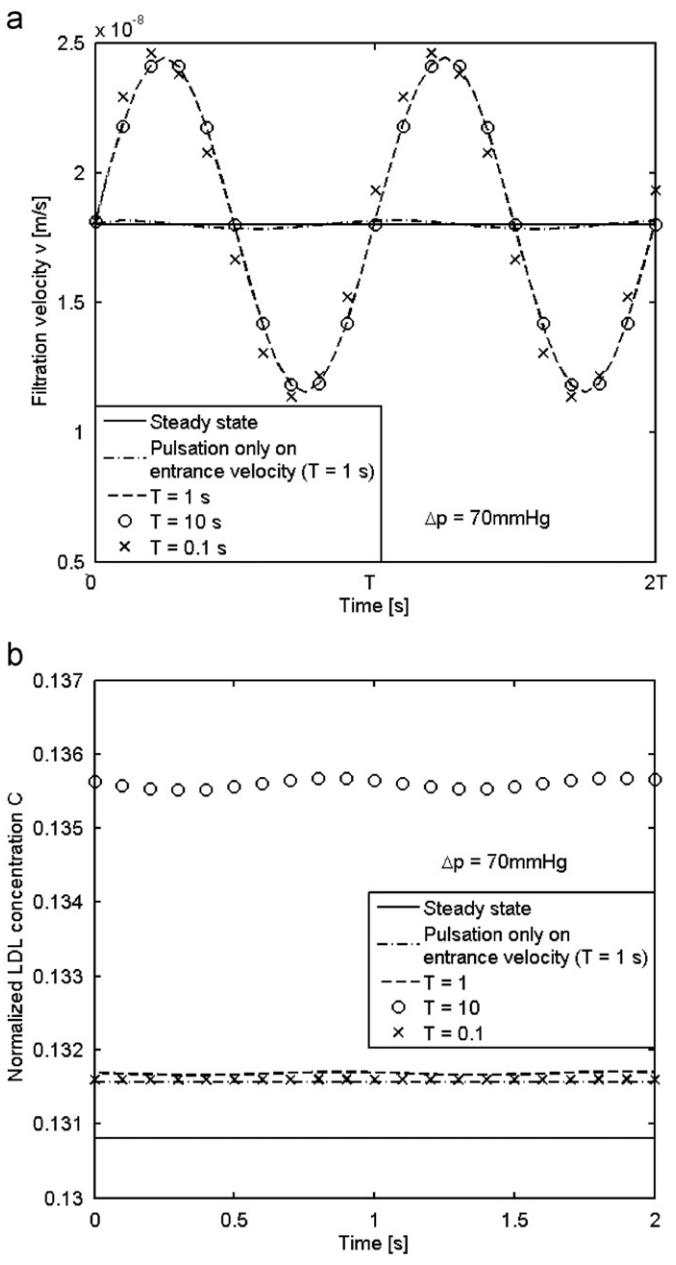

Fig. 16. (a) Filtration velocity and (b) normalized LDL concentration at different pulsation periods.

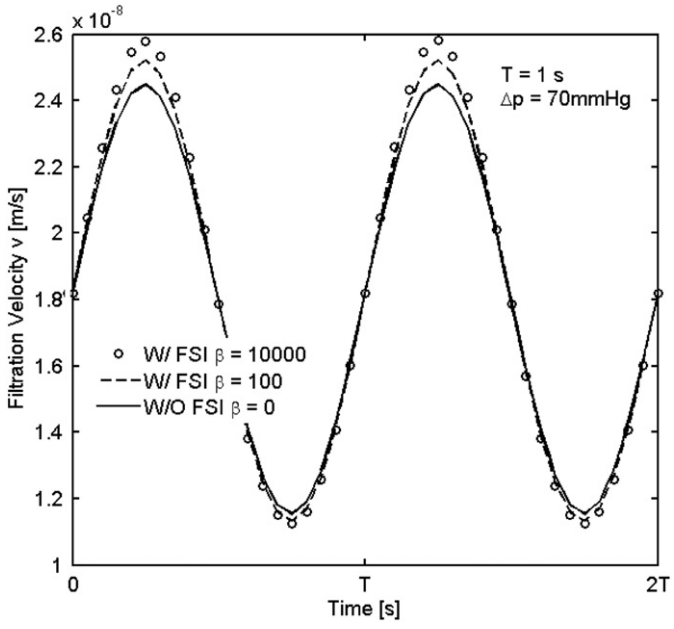

Fig. 17. Effect of FSI on filtration velocity incorporating the pulsation at the mid-axial position of the endothelium layer.

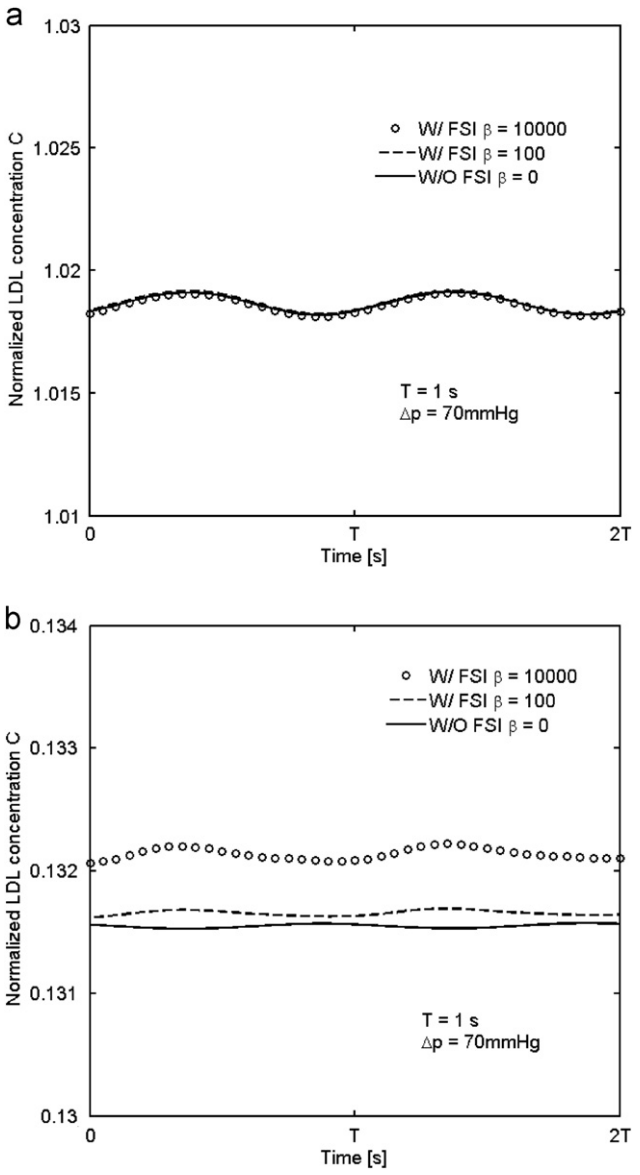

Fig. 18. Effect of FSI on normalized LDL concentration incorporating the pulsation at the (a) mid-axial position of the lumen–endothelium interface and (b) mid-axial position of the endothelium–intima interface.

5. Conclusions

A comprehensive model, which incorporates the multi-layer features as well as Fluid–Structure Interactions (FSI) for investigating LDL transport is analyzed and presented here. The presented model and the computational results are in excellent agreement with prior results. The presented model incorporates coupling of LDL transport and FSI and accounts for the elastic deformation of endothelium. Pore theorem is utilized to relate pore structure with hydraulic and mass-transfer parameters. Under steady state conditions, there is a significant impact from FSI on LDL concentration but a minor effect on filtration velocity. When pulsation effects are taken into account, the impact of FSI is quite minor due to the time period for the blood pulsation.

Conflict of interest statement

None.

References

Ai, L., Vafai, K., 2006. A coupling model for macromolecule transport in a stenosed arterial wall. International Journal of Heat and Mass Transfer 49, 1568–1591.
Curry, F.E., 1984. Mechanics and thermodynamics of transcapillary exchange. In: Handbook of Physiology. Microcirculation. The Cardiovascular System, Section. 2, vol. IV, Pt. 1, American Physiological Society, Bethesda, MD, pp. 309–374 (Chapter 8).
Fry, D.L., 1985. Mathematical models of arterial transmural transport. American Journal of Physiology 248, H240–H263.
Gao, F., Watanabe, M., Matsuzawa, T., 2006a. Stress analysis in a layered aortic arch model under pulsatile blood flow. Biomedical Engineering Online 5, 25.
Gao, F., Guo, Z.H., Sakamoto, M., Matsuzawa, T., 2006b. Fluid–structure interaction within a layered aortic arch model. Journal of Biological Physics 32, 435–454.
Huang, Y., Weinbaum, S., Rumschitzki, D., Chien, S., 1992. A fiber matrix model for the growth of macromolecular leakage spots in the arterial intima. Advances in Biological Heat and Mass Transfer HTD 231, 81–92.
Huang, Y., Rumschitzki, D., Chien, S., Weinbaum, S., 1994. A fiber matrix model for the growth of macromolecular leakage spots in the arterial intima. Journal of Biomechanical Engineering 116, 430–445.
Huang, Y., Rumschizki, D., Chien, S., Weinbaum, S., 1997. A fiber matrix model for the filtration through fenestral pores in a compressible arterial intima. American Journal of Physiology 272, 2023–2039.
Huang, Z.J., Tarbell, J.M., 1997. Numerical simulation of mass transfer in porous media of blood vessel walls. American Journal of Physiology 273, H464–H477.
Karner, G., Perktold, K., Zehentner, H.P., 2001. Computational modeling of macromolecule transport in the arterial wall. Computer Methods in Biomechanical and Biomedical Engineering 4, 491–504.
Kedem, O., Katchalsky, A., 1958. Thermodynamic analysis of the permeability of biological membranes to non-electrolytes. Biochimica et Biophysica Acta 27, 229–246.
Khanafer, K., Berguer, R., 2009. Fluid–structure interaction analysis of turbulent pulsatile flow within a layered aortic wall as related to aortic dissection. Journal of Biomechanics 42, 2642–2648.
Khanafer, K., Bull, J.L., Berguer, R., 2009. Fluid–structure interaction of turbulent pulsatile flow within a flexible wall axisymmetric aortic aneurysm model. European Journal of Mechanics B—Fluids 28, 88–102.
Meyer, G., Merval, R., Tedgui, A., 1996. Effects of pressure-induced stretch and convection on low-density lipoprotein and albumin uptake in the rabbit aortic wall. Circulation Research 79 (3), 532–540.
Michel, C.C., Curry, F.E., 1999. Microvascular permeability. Physiological Reviews 79, 703–761.
Moore, J.A., Ethier, C.R., 1997. Oxygen mass transfer calculations in large arteries. Journal of Biomechanical Engineering 119, 469–475.
Prosi, M., Zunino, P., Perktold, K., Quarteroni, A., 2005. Mathematical and numerical models for transfer of low-density lipoproteins through the arterial walls: a new methodology for the model set up with applications to the study of disturbed luminal flow. Journal of Biomechanics 38, 903–917.
Rappitsch, G., Perktold, K., 1996. Pulsatile albumin transport in large arteries: a numerical simulation study. Journal of Biomechanical Engineering 118, 511–519.
Stangeby, D.K., Ethier, C.R., 2002a. Coupled computational analysis of arterial LDL transport—effects of hypertension. Computer Methods in Biomechanical and Biomedical Engineering 5, 233–241.
Stangeby, D.K., Ethier, C.R., 2002b. Computational analysis of coupled blood–wall arterial LDL transport. Journal of Biomechanical Engineering 124, 1–8.
Tarbell, J.M., 2003. Mass transport in arteries and the localization atherosclerosis. Annual Review of Biomedical Engineering 5, 79–118.
Tada, S., Tarbell, J.M., 2004. Internal elastic lamina affects the distribution of macromolecules in the arterial wall: a computational study. American Journal of Physiology 287, H905–H913.
Truskey, G., Roberts, W., Herrmann, R., Malinauskas, R., 1992. Measurement of endothelial permeability to ^{125}I-low density lipoproteins in rabbit arteries by use of en face preparations. Circulation Research 7 (4), 883–897.
Wada, S., Karino, T., 2000. Computational study on LDL transfer from flowing blood to arterial walls. In: Yamaguchi, T. (Ed.), Clinical Applications of Computational Mechanics to the Cardiovascular System, Springer, Berlin, pp. 157–173.
Weinbaum, S., Tsay, R., Curry, F.E., 1992. A three-dimensional junction-pore-matrix model for capillary permeability. Microvascular Research 44, 85–111.
Wen, G.B., Weibaum, S., Ganatos, P., Pfeffer, R., Chien, S., 1988. On the time dependent diffusion of macromolecules through transient open junctions and their subendothelial spread. 2. Long time model for interaction. Journal of Theoretical Biology 135, 219–253.
Yang, N., Vafai, K., 2006. Modeling of low-density lipoprotein (LDL) transport in the artery—effects of hypertension. International Journal of Heat and Mass Transfer 49, 850–867.
Yang, N., Vafai, K., 2008. Low-density lipoprotein (LDL) transport in an artery—a simplified analytical solution. International Journal of Heat and Mass Transfer 51, 497–505.
Yuan, F., Chien, S., Weinbaum, S., 1991. A new view of convective–diffusive transport processes in the arterial intima. Journal of Biomechanical Engineering 133, 314–329.